Hindawi Publishing Corporation
Mathematical Problems in Engineering
Volume 2016, Article ID 8024043, 11 pages
http://dx.doi.org/10.1155/2016/8024043

Research Article

Buckling Instability Behavior of Steel Bridge under Fire Hazard

Ying Wang and Muyu Liu

Hubei Key Laboratory of Roadway Bridge & Structure Engineering, Wuhan University of Technology, Wuhan 430070, China

Correspondence should be addressed to Muyu Liu; liumuyu@whut.edu.cn

Received 28 December 2015; Accepted 24 March 2016

Academic Editor: Veljko Milutinovic

Failure of buckling instability will most likely occur before the displacement reaches the allowable value of the code when a tanker burns under the steel bridge. This research focuses on critical buckling stress of bridge under fire hazard and a thermal analysis model of a steel bridge is established by FDS (Fire Dynamics Simulator). Thermal parameters of the steel are determined by the polynomial fitting method. Temperature field and elastic modulus of the bridge changing with time are calculated by determining the heat release rate function of tanker. Critical buckling stress of the bridge web and bottom floor changing with time is calculated according to steel floor buckling theory. Finite element software ANSYS is used to verify the result. Results show that when a tanker is burning for 17 minutes, critical buckling stress of steel web will be reduced to $\tau_{crl,lw}(T) = 19.1$ MPa and $\sigma_{crl,lw}(T) = 38.8$ MPa, which is less than the web stress ($\tau = 19.6$ MPa, $\sigma = 39.8$ MPa) caused by dead and live load. So steel web will be the first to show shear flexural bending buckling failure. Displacement in the midspan will reach 35.4 mm at this time, which was less than the allowable displacement (50 mm) set by standard. The best rescue time of the bridge under fire hazard is within 15 minutes.

1. Introduction

City viaduct and overpass were the key components of modern transportation. Once fire hazard occurred, it would cause great losses. On April 29, 2007, a tanker carrying about 32 thousand and 600 liters of gasoline crashed into a landmark tower on the highway overpass and then overturned in Michigan [1]. The bridge was bending by the heat generated by the fire that resulted in 250-meter-long bridge collapse. The elastic modulus of floor would decrease rapidly with the increase of temperature when steel bridge was under fire hazard, leading to serious deformation or collapse during fire. It was likely that the failure of buckling instability of the steel bridge would occur before the displacement reached the allowable value of the code under fire hazard. Therefore, it was important to study the temperature variation and buckling characteristics of the steel bridge under fire hazard.

In recent years, some scholars began to study the transient temperature field and the mechanical properties of steel bridge under fire because of its tremendous harm. Garlock et al. [1] presented a detailed review of actual fire incidents, case studies related to fire hazards, and postfire assessment and repair strategies in bridges. The study pointed out that the number of damaged bridges caused by fire is nearly 3 times more than that caused by earthquake. Kodur and Naser [2] analyzed the mechanical properties of the steel-concrete composite beam bridge under high temperature by the method of heating curve. The research showed that fire resistance performance of steel-concrete composite beam bridge was much better than the steel bridge. Transient temperature field and the failure mode of the steel-concrete composite bridges under fire were studied by means of finite element method and verified by experiments [3]. Mechanical behavior of simply supported beam bridge under fire was analyzed by ANSYS [4]. Relationship between displacement of midspan and time was presented under fire and finally the bridge's destruction time was obtained.

In current fire resistance study of bridge, most researchers considered that the bridge would be damaged when displacement of the bridge under fire is exceeding the allowable value of the code [5, 6]. But for the steel bridge, critical buckling stress of bridge would be reduced greatly due to rapid increase of temperature and decrease of elastic modulus. Therefore, it was likely that buckling failure would

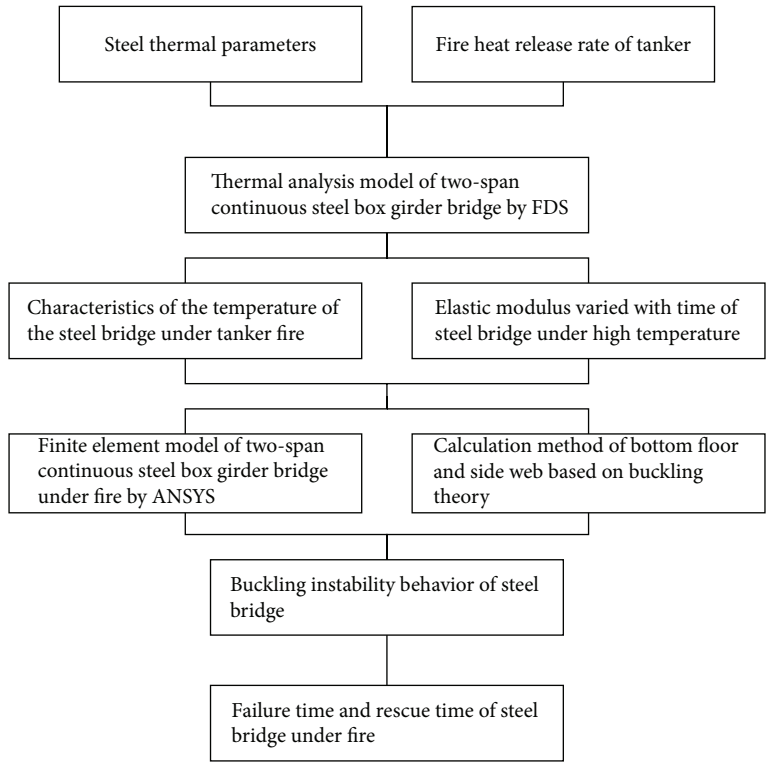

Figure 1: Conceptual scheme of buckling instability behavior of steel bridge under fire hazard.

occur before the displacement of bridge reaches the allowable value of the code. In this study, the critical buckling stress variation of the web and the bottom floor of steel bridge was analyzed and failure time of steel bridge under high temperature was obtained. Results showed that the failure of buckling instability occurred before the displacement in midspan reached the allowable value of the code of the steel bridge under fire hazard. The best rescue time of bridge was obtained and this can provide reference for bridge fire resistance design. Conceptual scheme of buckling instability behavior of steel bridge under fire hazard is shown in Figure 1.

2. Project Summary

The bridge researched in this study is a 2 × 30 m continuous steel girder bridge located in Wuhan, Hubei, China, Gusao tree overpass of Tianhe District Second Highway Engineering. Vertical clearance under the bridge is 4 m and the height of the girder is 1.68 m, as shown in Figure 2(a). The position in which tanker fire happened is shown in Figure 2(b).

Material of the bridge is steel Q370qD [7]. The yield strength (fy) of steel Q370qD is 370 MPa and the elasticity modulus (E) of steel Q370qD is 210 GPa at room temperature. The top of girder width is 9 m and the height of girder at the design of line is 1.68 m, both sides of the cantilever box girder are 1.75 m long, cantilever root height is 0.5 m, and end height is 0.25. Number and dimensions of the different groups of ribs are shown in Table 1. Cross-sectional layout of the bridge is shown in Figure 3.

3. Steel Thermal Parameters and Fire Heat Release Rate

3.1. Expressions for the Steel Thermal Parameters. The thermal parameters used in this study include thermal conductivity (W/(m·K)), specific heat (J/(kg·K)), thermal expansion coefficient, and elastic modulus (MPa). Thermal parameters of steel vary with temperature observably, and the value of the research results is relatively discrete. Therefore, this study firstly summarizes the value of thermal parameters in [8–11]. Then, according to the principle of least square method, thermal parameters are fitted by polynomial fitting to minimize the value error. The polynomial fitting expressions of thermal parameters are obtained as follows.

Cubic polynomial fitting of thermal conductivity of steel is obtained as

$$\lambda = 2.15 \times 10^{-8} T^3 - 4.22 \times 10^{-5} T^2 - 1.03 \times 10^{-2} T + 51.08. \quad (1)$$

Quadratic polynomial fitting of specific heat of steel is obtained as

$$c = 4.64 \times 10^{-4} T^2 + 11.3 \times 10^{-2} T + 486.37. \quad (2)$$

Linear polynomial fitting of thermal expansion coefficient of steel is obtained as

$$\alpha = 9.10 \times 10^{-9} T + 1.08 \times 10^{-5}. \quad (3)$$

Table 1: Dimensions of steel box girder.

Position	Thickness	Type of stiffeners	Thickness of stiffeners	Number of stiffeners
Top flange	20 mm, 24 mm	T-rib	Web of 12 mm, flange of 10 mm	22
Bottom flange	20 mm, 24 mm	T-rib	Web of 12 mm, flange of 10 mm	14
Side web	16 mm	Rib plate	12 mm	9
Middle web	16 mm	Rib plate	12 mm	3
Diaphragm	12 mm	—	—	—

Note: the spacing of the diaphragm is 1.5 m in the longitudinal direction of the bridge.

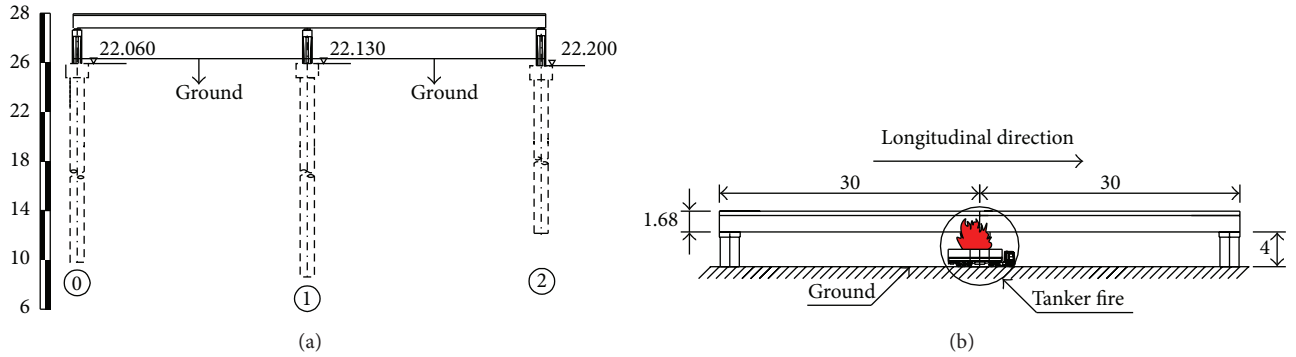

Figure 2: (a) Overpass of Tianhe District Second Highway Engineering in Wuhan city (m). (b) Position in which tanker fire happened (m).

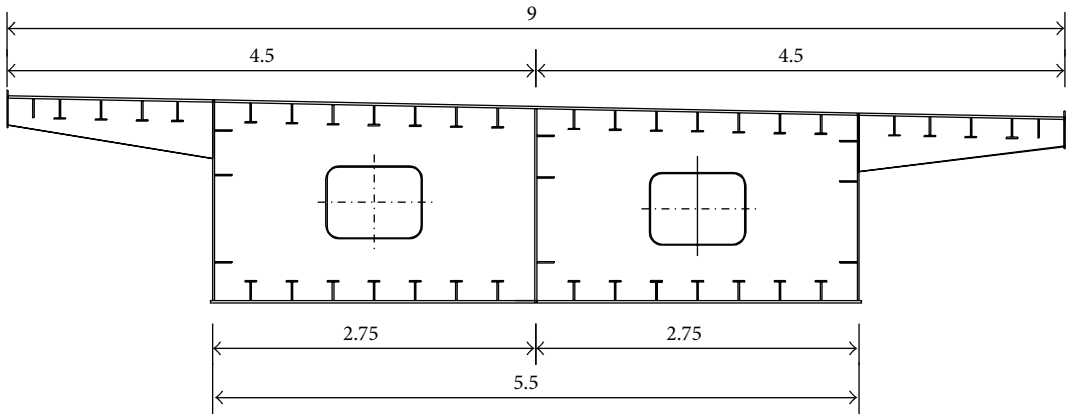

Figure 3: Cross-sectional layout of steel box girder bridge (m).

Polynomial fitting of elastic modulus of steel is obtained as

$$\frac{E(T)}{E} = 3.55 \times 10^{-18} T^6 - 2.07 \times 10^{-14} T^5 + 4.00 \times 10^{-11} T^4 - 3.16 \times 10^{-8} T^3 + 9.02 \times 10^{-6} T^2 - 0.0014T + 1.038, \quad (4)$$

where T is temperature (°C).

Thermal parameters varied with time are shown in Figure 4. E is elastic modulus of steel at room temperature and $E(T)$ is elastic modulus of steel at temperature T°C. In Figure 4(d), the steel Q370qD loses almost all of its elastic modulus between 1000°C and 1200°C. In the range between 1000°C and 1200°C, elastic modulus of steel is close to 0. So polynomial fitting curve of elastic modulus presents a horizontal trend between 1000°C and 1200°C.

3.2. Heat Release Rate Function. Heat release rate growth models are widely studied in the field of tunnel and some scholars studied the heat release rate growth models based on the fire experiment in tunnel in the past few years. There are many kinds of fire heat release rate growth models to analyze fire hazard. Linear growth model, square growth model, and exponential growth model are usually used. The growth model is composed of two parts: the maximum heat release rate (Q_{max}) and the recession function [12].

The whole process of fire heat release rate is basically reflected through these heat release rate growth models. Linear model is simplest in the mathematical model of heat release rate and there are large deviations with the growth

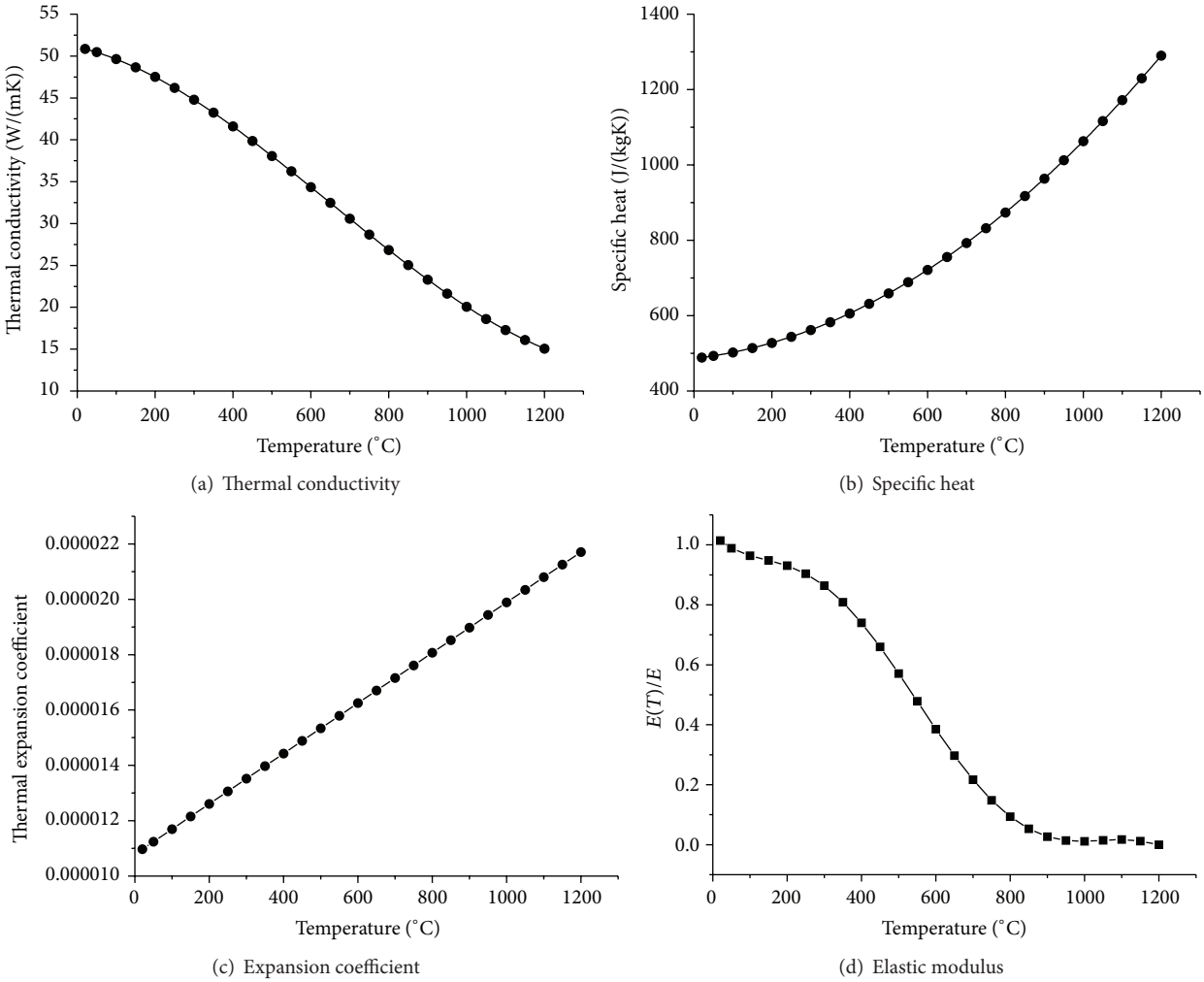

(a) Thermal conductivity

(b) Specific heat

(c) Expansion coefficient

(d) Elastic modulus

Figure 4: Polynomial fitting curve of steel thermal parameters.

curve of the actual fire heat release rate. The mathematical model of the heat release rate under different control conditions is given by exponential model, and the growth curve is also most consistent with the actual fire. In this study, the exponential growth model is used to model the fire heat release rate.

The heat release model of the exponential heat release rate fire is given by

$$\mathrm{HRR} = Q_{\max} \cdot n \cdot r \cdot \left(1 - e^{-k \cdot t}\right)^{n-1} \cdot e^{-k \cdot t}, \tag{5}$$

where HRR is the heat release rate function (MW), Q is the maximum heat release rate (MW), n, r, and k are parameters under different fire scenarios, and t is the fire time (s).

Seven kinds of heat release rate models under fire scenarios are given by foreign research [13], as shown in Table 2, and the corresponding fire heat release rate curve is shown in Figure 5. There is very little current research on bridges in fire, but characteristic of fuel combustion in the bridge is similar to that in the tunnel. This research takes some tunnel fire curves as a consequence of the absence of bridge fire curves.

From Figure 5, the heat release rate peak of scenario 7 is too high, and its temperature growth rate is much faster than other scenes. This fire scale is most dangerous. Therefore, the fire scene used in this study is a 200 MW oil tanker burning near steel bridge.

4. Results of Thermal Analysis Model

4.1. Thermal Analysis Model. The thermal analysis model of two-span continuous steel box girder bridge is established by FDS (Fire Dynamics Simulator). In this research, the employed version of FDS is FDS 5.0. FDS was developed by NIST (National Institute of Standards and Technology) in America. FDS is a powerful fire simulator and FDS simulates fire scenarios using computational fluid dynamics (CFD) optimized for low-speed, thermally driven flow. This approach is very flexible and can be applied to fires ranging from stove-tops to oil storage tanks. FDS models can predict smoke, temperature, carbon monoxide, and other substances during fires. The results of these simulations have been used to ensure the safety of structures before construction.

Table 2: The value of fire heat release rate exponential growth model.

Fire scenarios	Fire type	Total heat energy E_{tot} (GJ)	Maximum heat release rate Q_{max} (MW)	n	r	$k(*10^{-3})$
1	Two cars	14.4	8	2.1	2.04	1.13
2	Bus	52.5	25	2.0	2.0	0.95
3	Truck + bus	75	75	5	2.44	2.44
4	Heavy truck (low exposure)	150	100	3.2	2.28	1.52
5	Heavy truck (high exposure)	225	150	3.2	2.28	1.52
6	Truck + bus + 6 cars	367	175	2.6	2.17	1.04
7	Tanker	1500	200	1.1	1.27	0.17

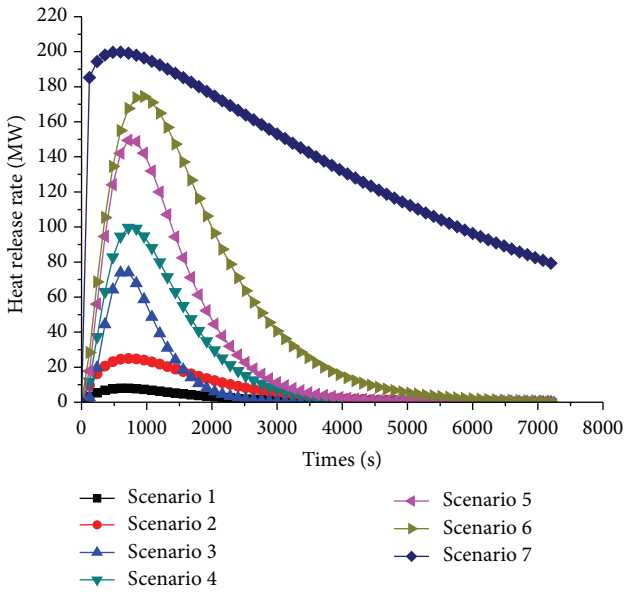

Figure 5: Heat release curves under different fire scenes.

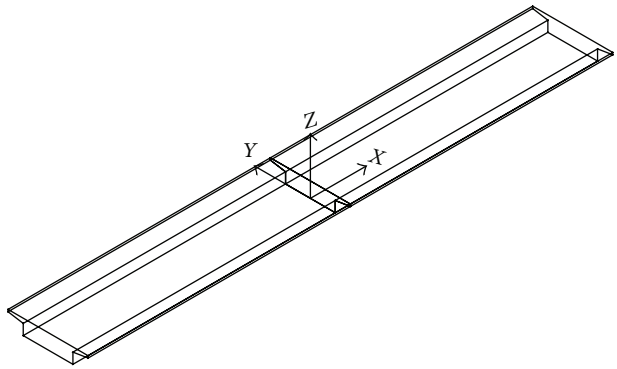

Figure 6: Coordinate axis of thermal analysis model.

FDS model validation was proved by many researchers. Alos-Moya et al. researched a bridge failure due to fire using computational fluid dynamics and finite element models and pointed out that FDS models were able to simulate the observed response of the bridge under fire hazard [14].

In the bridge model, the coordinate axis center is located in the center line of the base floor of bridge abutment, the longitudinal direction of the bridge is x direction, transverse direction of the bridge is Y direction, and z direction is vertical, as shown in Figure 6.

The calculation area of X direction is 80 m, divided into 80 segments. The Y direction is 15 m, divided into 45 segments. The Z direction is 10 m, divided into 50 segments. The whole computing model is divided into 180000 mesh.

In this FDS model, two kinds of sensors are used. Thermocouples are set up to measure gas temperature and wall sensors are set up to measure bridge temperature. The initial temperature is set at 20°C, and the wind speed is not considered. The cross-sectional temperature measuring points arrangement of steel box girder is shown in Figure 7 to measure transient temperature variation of bridge under tanker burning. Because the cross section is symmetrical along the centerline, test points are only arranged on $+Y$ direction. Wall sensors are set up in the girder to measure the temperature of each part. The bottom floor has 10 test points, from D1 to D10, spacing 300 mm. The roof floor has 8 test points, from D11 to D18, spacing 600 mm. The outer web has 8 test points, from F1 to F8, spacing 200 mm. The inner web has 8 test points, from F9 to F16, spacing 200 mm.

Bottom floor in negative moment area is in the state of compression and the side web is in the state of bending shear stress. Negative moment area webs are most prone to instability for that web critical buckling stress in negative moment area is far less than the other position and the temperature of the side web and the bottom floor rises fastest under hazard. So the fire source is located in negative moment area. The fire is set to 12 m long, 2 m wide 200 MW tanker. Fire is 4 m under the bridge because clearance height of bridge is 4 m. Fire center coordinates are (0, 0, −4 m). The heat release rate (MW) function is

$$\mathrm{HRR} = 200 \times 1.1 \times 1.27 \times \left(1 - e^{-0.00017 \cdot t}\right)^{1.1-1} \times e^{-0.00017 \cdot t}. \quad (6)$$

In this paper, special value for soot yield was considered in the FDS model. In the FDS model, soot yield changes with the heat release rate of oil tanker. Heat release rate of oil tanker was defined as the source of fire, and soot yield could vary with heat release rate. Temperature of soot would transfer towards the bridge through convection radiation.

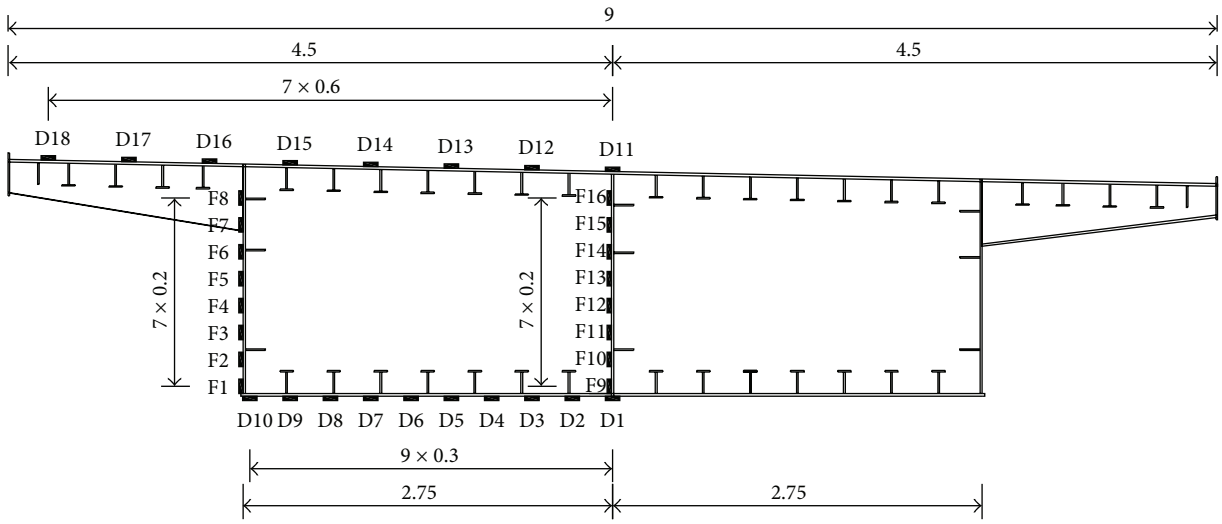

Figure 7: Temperature measuring point arrangement of steel box girder (m).

So temperature of steel would change with time due to the tanker fire and soot yield.

4.2. Results of Thermal Analysis. In this research, abutments of the bridge use concrete C50. Elasticity modulus of C50 is 3.45×10^4 MPa at room temperature. Thermal conductivity of C50 is 1.52 W/(m·K) at room temperature. Thermal conductivity of deck of the bridge (steel Q370qD) is 51 W/(m·K) at room temperature. Thermal conductivity of abutments is far less than thermal conductivity of deck of the bridge. That means abutments have poor thermal conductive ability. When fire happens, heating rate of abutments is very slow. Temperature of abutments is very low and it is far less than temperature of the deck of the bridge. Mechanical properties of abutments change little under fire. So in this paper, calculation of abutments does not need to be done under fire.

Temperature of the steel bridge in the process of the continuous 60-minute combustion is increasing rapidly. Transient temperature of steel girder, the heat flux density, and transient temperature of surrounding air are calculated.

Wall sensors are set up in the girder to measure the temperature of each part. The calculation results show that temperature from D1 to D10 has little difference, so as F1 to F8, F9 to 16, and D11 to D18. So in this paper, the average temperature of bottom floor, the average temperature of middle web, the average temperature of side web, and the average temperature of top floor were used to calculate the buckling stresses of the girder.

By taking the average temperature of bottom floor, middle web, side web, and top floor, the average temperature of the corresponding parts is obtained, as shown in Figure 8.

When fire hazard happens, source of fire would burn and release heat first. As a result, heat release rate would increase. Then temperature of the air around fire would increase based on the heat. Air around fire then transfers heat to the bridge through convection and radiation. As a result, temperature of bridge would increase. Temperature rising rate of bridge lags behind fire heat release rate for that it takes some time for the bridge temperature to rise during convection and radiation. In Figure 8, temperature maintains a horizontal trend between 1200 s and 3600 s. In Figure 5, when time reaches 1200 s, the heat release rate drops to about 180 MW, and when time reaches 3600 s, the heat release rate drops to about 150 MW; 150 MW~180 MW has enough heat to let the bridge temperature maintain a horizontal trend. So Figure 8 shows curves with no decay. If the heat release rate drops to some value which is very low (e.g., under 100 MW) over time, Figure 8(d) may decay.

From the graph, the temperature of the bottom floor and the side web under fire rose rapidly and reached the highest temperature. The highest temperature of bottom floor exceeded 1000°C. The highest temperature of top floor and middle web was relatively low, and highest temperature of middle web was close to 600°C. Each part of the warming trend is consistent, and the highest temperature is about 20 minutes.

The elastic modulus of steel at high temperature will change greatly. According to formula (4), the elastic modulus of bottom floor, middle web, side web, and top floor under high temperature is obtained, as shown in Figure 9.

5. Buckling Stress Calculation Method for Steel under High Temperature

From Figure 8, temperature of side web is much higher than that of middle web. So side web is more dangerous than middle web. Therefore, the critical bending shear buckling stress expression of the side web and the critical buckling stress of the stiffened bottom floor bearing axial pressure under variation temperature are derived, respectively.

Elastic stability theory of steel floor is used in this section. The critical bending shear buckling stress expression of the side web and the critical buckling stress of the stiffened bottom floor bearing axial pressure under variation temperature

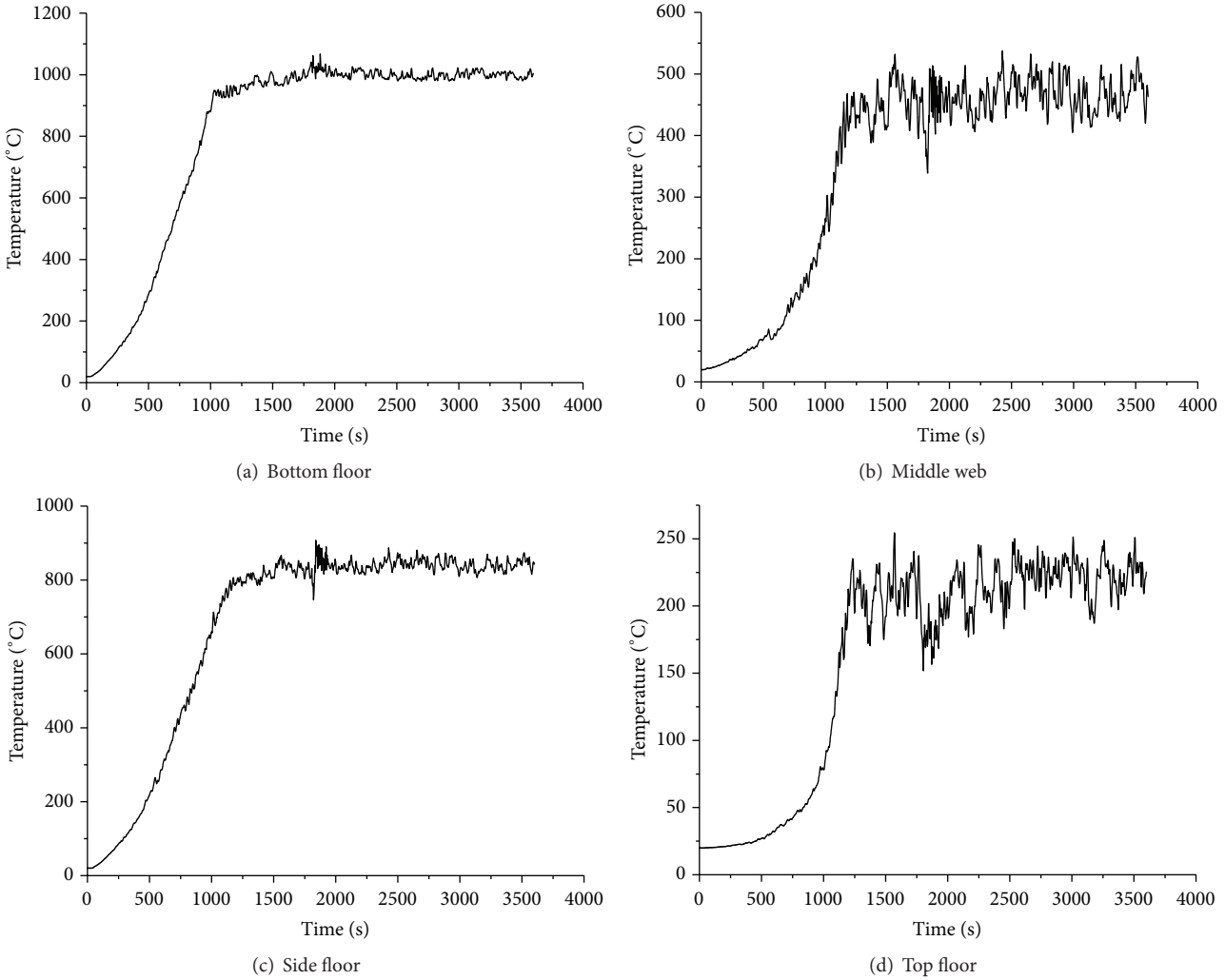

Figure 8: Average temperature varied with time of steel bridge.

are derived, respectively [15–17]. The concrete derivation process is as follows.

5.1. Calculation Method of Bottom Floor Based on Buckling Theory. The area ratio δ_l of the bottom floor is the ratio of the area of a rib A_l to the area of floor section $b \times t$:

$$\delta_l = \frac{A_l}{bt} = \frac{100 \times 10 + 160 \times 12}{350 \times 20} = 0.417. \quad (7)$$

The stiffness ratio γ_l of the bottom floor is the ratio of bending rigidity EI_l of connection position of stiffer and floor to product of D and floor width b:

$$\gamma_l = \frac{\mathrm{EI}_l}{Db} = \frac{12I_l\left(1-\upsilon^2\right)}{t^3 b} = \frac{12 \times 41992333 \times \left(1-0.3^2\right)}{350 \times 20^3} = 163, \quad (8)$$

where υ is Poisson's ratio, t is floor thickness, and b is stiffened floor width.

According to [12], the stiffer is rigid when the aspect ratio of the stiffened floor meets condition $\alpha \le \alpha_0$:

$$\gamma_l^* = \frac{1}{n}\left[4n^2\left(1+n\delta_l\right)\alpha^2 - \left(\alpha^2+1\right)^2\right] = \frac{1}{8}\left[4 \times 8^2\left(1+8\times 0.417\right)0.582^2 - \left(0.582^2+1\right)^2\right] = 46.78, \quad (9)$$

where $\alpha_0 = \sqrt[4]{1+(n+1)\gamma_l} = \sqrt[4]{1+(8+1)163} = 6.19$.

$a = 1600$, and a is width of subplate divided by stiffeners.

$b = 2750$, and b is length of subplate divided by stiffeners.

$\alpha = a/b = 1600/2750 = 0.582$; N is the number of web segmentations.

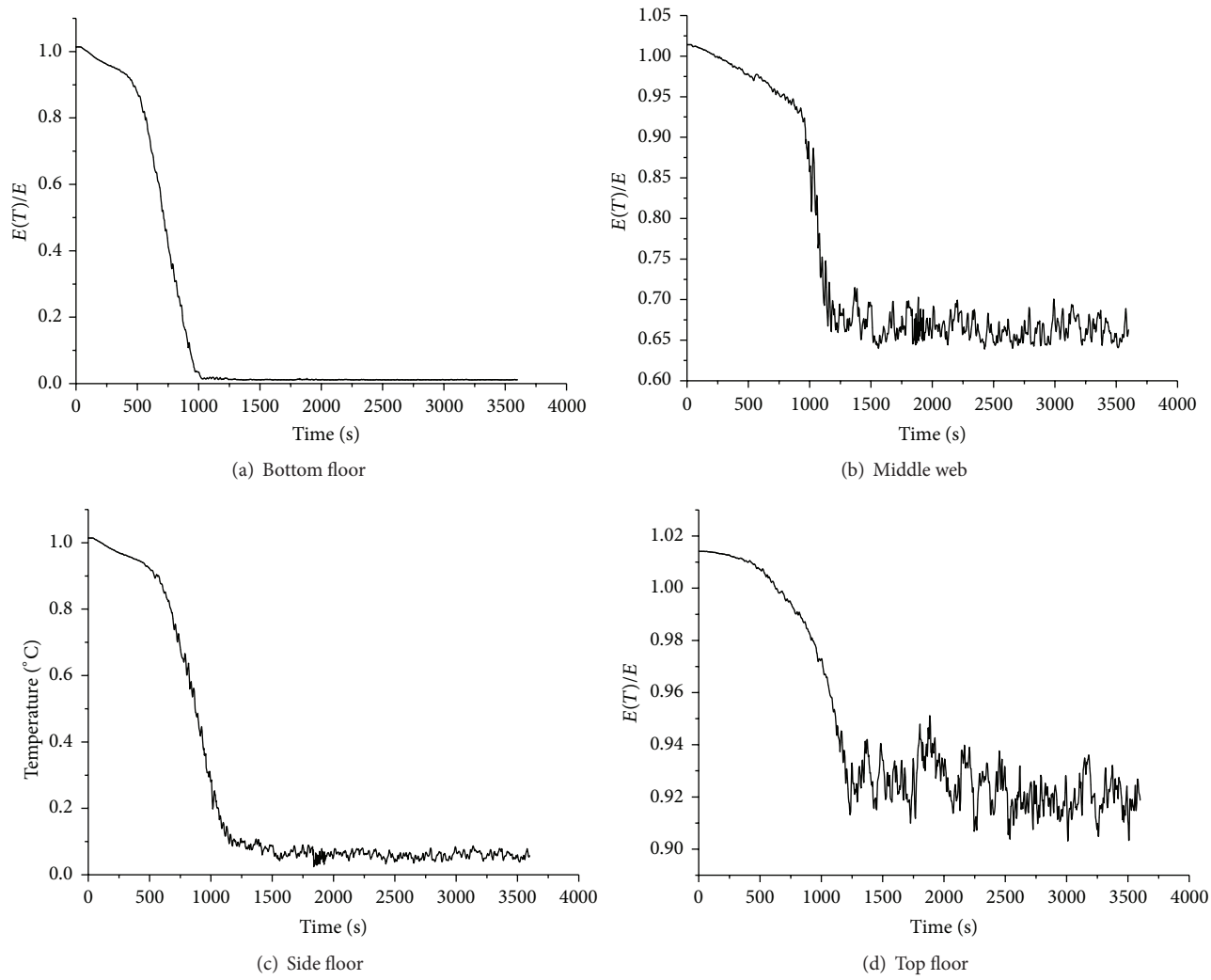

Figure 9: Elastic modulus varied with time of steel bridge.

So the bottom floor stiffener is rigid, and the critical buckling stress coefficient for bottom floor stiffener without considering the constraints of the web on the bottom is

$$k = 4(n+1)^2 = 324. \tag{10}$$

Therefore, the critical buckling stress of bottom stiffened floor under room temperature is

$$\sigma_{\text{crl}} = \frac{\pi^2 E (n+1)^2 t^2}{3(1-v^2) b^2} = 3187\ \text{MPa}. \tag{11}$$

From this, it is seen that the critical buckling stress of the bottom floor is a function related to the elastic modulus E of steel. When fire hazard happens, bottom floor is directly affected by the fire temperature, and the bottom floor is heated. The elastic modulus of bottom stiffening rib is decreased. According to the change function of elastic modulus and temperature of steel of (4), it can be seen that

$$\sigma_{\text{crl}}(T) = \frac{\pi^2 E(T) (n+1)^2 t^2}{3(1-v^2) b^2}. \tag{12}$$

The bridge will be suddenly destroyed due to high temperature buckling, when $\sigma_{\text{crl}}(T)$ is less than the actual stress of floor, causing serious consequences such as bridge collapse. The critical buckling stress of bottom floor when fire is burning for 17 minutes is $\sigma_{\text{crl}}(T) = 51$ MPa according to (4) and (12).

5.2. Calculation Method of Side Web Based on Buckling Theory. Derivation process of calculation method of web buckling is very complicated. Derivation process contains a large number of differentials and integrals. So we give the critical buckling stress of web under bending load and under shear load based on [15]. The detailed derivation process is in [15].

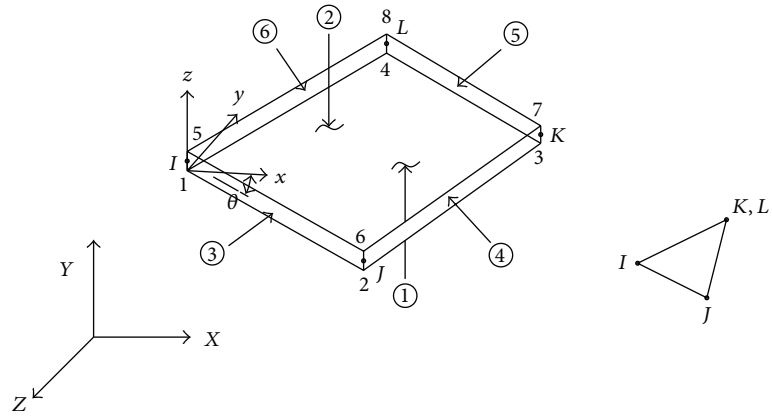

Figure 10: Shell63 geometry.

Critical buckling stress of side web under bending load is

$$\sigma_{\mathrm{crl},lw} = \frac{\pi^2 E k t_w^{\,2}}{12\left(1-v^2\right) h_w^{\,2}}. \tag{13}$$

When $a_w > h_w$, it can be seen as follows:

$$\psi = \frac{\sigma_2}{\sigma_1} = -0.5, \qquad k = 7.81 - 6.29\psi + 9.78\psi^2, \tag{14}$$

$$\sigma_{\mathrm{crl},lw}(T) = \frac{\pi^2 E(T) k t_w^{\,2}}{12\left(1-v^2\right) h_w^{\,2}}, \tag{15}$$

where ψ is bending gradient and a_w, h_w, and t_w are the width, height, and thickness of floor, respectively.

Critical buckling stress of side web under shear load is

$$\tau_{\mathrm{crl},lw} = \frac{\pi^2 E k t_w^{\,2}}{12\left(1-v^2\right) a_w^{\,2}}, \qquad k = \begin{cases} 5.34 + 4.0\left(\dfrac{h_w}{a_w}\right)^2 & \left(a_w > h_w\right), \\ 4.0 + 5.34\left(\dfrac{h_w}{a_w}\right)^2 & \left(a_w \le h_w\right), \end{cases} \tag{16}$$

$$\tau_{\mathrm{crl},lw}(T) = \frac{\pi^2 E(T) k t_w^{\,2}}{12\left(1-v^2\right) a_w^{\,2}}.$$

Web critical buckling stress under bending shear stress station should meet the condition of

$$\left(\frac{\sigma}{\sigma_{\mathrm{crl},lw}(T)}\right)^2 + \left(\frac{\tau}{\tau_{\mathrm{crl},lw}(T)}\right)^2 \le 1. \tag{17}$$

Web critical buckling stress theoretical value under room temperature is $\tau = 80.3$ MPa, $\sigma = 167.1$ MPa from (15) and (16) and web critical buckling stress is $\tau = 18.5$ MPa, $\sigma = 38.4$ MPa when tanker fire is burning for 17 minutes.

6. Buckling Instability Finite Element Analysis of Steel Bridge under Fire

The fine steel shell model is established to get center span deflection under high temperature, bending share ratio, and bending stress gradient because the bending share ratio and bending stress gradient of the bridge are unknown. The validity of the theoretical formula is verified by establishing independent web and stiffening floor model. The finite element software ANSYS [18] is used to establish the model of two-span continuous steel bridge, and the element type of steel beam is shell63. There are 63254 units and 102458 nodes among the whole bridge. The version of ANSYS is ANSYS 14.0 in this research.

Shell63 has both bending and membrane capabilities. Both in-plane and normal loads are permitted. The element has six degrees of freedom at each node: translations in the nodal x, y, and z directions and rotations about the nodal x-, y-, and z-axes. Stress stiffening and large deflection capabilities are included. A consistent tangent stiffness matrix option is available for use in large deflection (finite rotation) analyses.

Temperatures may be input as element body loads at the "corner" locations (1–8) shown in Figure 10: "shell63 geometry." The first corner temperature T1 defaults to TUNIF. If all other temperatures are unspecified, they default to T1. If only T1 and T2 are input, T1 is used for T1, T2, T3, and T4, while T2 (as input) is used for T5, T6, T7, and T8. For any other input pattern, unspecified temperatures default to TUNIF, as shown in Figure 10.

Gravitational acceleration in this paper is 9.8 m/s^2. The density of steel is 7850 kg/m^3. Gravity loads of the bridge are 3560 kN.

The buckling mode, web shear stress, and web and bottom stress of the bridge under room temperature are calculated under the action of dead load and lane load.

From the calculation results, it is seen that the bending stress gradient of web is −8.5 MPa/(36.8 MPa).

The side web model is established independently surrounded by simply supported sides because its heating rate is far greater than middle floor and the highest temperature

Table 3: Floor stress when tanker is burning for 17 minutes.

Floor position	Actual stress	Theoretical value of critical buckling stress	Finite element value of critical buckling stress
Side floor	$\tau = 19.6$ MPa	$\tau = 18.5$ MPa	$\tau_{cr1,lw}(T) = 19.1$ MPa
	$\sigma = 39.8$ MPa	$\sigma = 38.4$ MPa	$\sigma_{cr1,lw}(T) = 38.8$ MPa
Bottom floor	$\sigma = 37.1$ MPa	$\sigma_{cr1}(T) = 51.0$ MPa	$\sigma_{cr1}(T) = 65.7$ MPa

is far higher than middle floor according to the results of Figure 8. Bending shear ratio is 2.03 : 1 and bending gradient is −0.5. Critical buckling stress value from finite element calculation is $\tau = 95.9$ MPa, $\sigma = 193$ MPa.

Critical buckling stress of side web is $\tau = 92.3$ MPa, $\sigma = 187.3$ MPa; $\tau = 83.5$ MPa, $\sigma = 169.6$ MPa; $\tau = 44.3$ MPa, $\sigma = 89.9$ MPa; $\tau = 19.1$ MPa, $\sigma = 38.8$ MPa, when the fire is burning for 5 minutes, 10 minutes, 15 minutes, and 17 minutes, respectively, according to the elastic modulus of web changing with temperature under fire.

Stiffened bottom floor model is established independently surrounded by simply supported sides. Critical buckling stress of finite element calculation under uniform pressure and room temperature is $\sigma = 3025$ MPa.

Critical buckling stress of bottom floor is $\sigma = 2883$ MPa, $\sigma = 2240$ MPa, $\sigma = 445$ MPa, and $\sigma = 65.7$ MPa, when the fire is burning for 5 minutes, 10 minutes, 15 minutes, and 17 minutes, respectively, according to the elastic modulus of bottom floor changing with temperature under fire.

From finite element calculation, it is seen that critical buckling stress will be reduced to $\tau_{crl,lw}(T) = 19.1$ MPa, $\sigma_{crl,lw}(T) = 38.8$ MPa, when tanker is burning for 17 minutes and at this time critical buckling stress does not comply with (17). Therefore, the web will be the first to show bending shear buckling failure.

Critical buckling stress of bottom floor will be reduced to 65.7 MPa, when the fire is burning for 17 minutes, higher than actual stress $\sigma = 37.1$ MPa caused by dead and live load under high temperature. So bottom floor will not be destroyed in 17 minutes, as shown in Table 3.

Elastic modulus of each floor in the negative moment region is reduced by (4) to calculate the growth of displacement in midspan under fire load. Displacement values of the bridge are 21.2 mm, 25.7 mm, 31.5 mm, and 35.4 mm, when bridge is at room temperature, burning for 10 minutes, 15 minutes, and 17 minutes, respectively.

From displacement analysis, it is seen that displacement in midspan of steel bridge will increase, and the displacement will increase from 21.2 mm to 35.4 mm in 17 minutes, less than the allowable value of the code [19] (L/600 = 50 mm), where L is the length of the span.

The calculation results show that buckling instability of the side web of the steel bridge will be the first to occur before the allowable value of the bridge is reached.

7. Conclusions

(1) Thermal analysis model of two-span continuous steel girder bridge is established by fire dynamics software FDS. Thermal release rate function of tanker fire is obtained to simulate tanker burning. Transient temperature field and elastic modulus changing with time in the negative moment region of the bridge are calculated.

(2) Critical buckling stress of web and the bottom floor changing with time is obtained by calculating the buckling behavior of the bridge under high temperature of fire. Stress of side web is greater than the critical buckling stress under tanker burning for 17 minutes and the bending shear buckling failure will be the first to occur. At this time, displacement in midspan is still maintained within the allowable range of specifications.

(3) Temperature of web and bottom floor rises very fast when tanker burns for 15 minutes to 17 minutes, which is a very dangerous moment, while temperature of web and bottom floor is maintained at a relatively low level during the first 15 minutes, and the bridge has a large safety reserve. So the best rescue time of the steel bridge under tanker fire is within 15 minutes. The bridge is likely to be destroyed if the tanker burns more than 15 minutes.

Competing Interests

The authors declare that they have no competing interests.

Acknowledgments

This paper was financially supported by the National Natural Science Fund, "Stability of High Web in Long-Span Steel-Concrete Composite Bridge Based on the Elastic Rotational Restraint Boundary" (no. 51378405), and the Natural Science Fund of Hubei Province (no. 2013CFA049).

References

[1] M. Garlock, I. Paya-Zaforteza, V. Kodur, and L. Gu, "Fire hazard in bridges: review, assessment and repair strategies," *Engineering Structures*, vol. 35, pp. 89–98, 2012.

[2] V. K. R. Kodur and M. Z. Naser, "Importance factor for design of bridges against fire hazard," *Engineering Structures*, vol. 54, pp. 207–220, 2013.

[3] E. M. Aziz, V. K. Kodur, J. D. Glassman, and M. E. Moreyra Garlock, "Behavior of steel bridge girders under fire conditions," *Journal of Constructional Steel Research*, vol. 106, pp. 11–22, 2015.

[4] I. Payá-Zaforteza and M. E. M. Garlock, "A numerical investigation on the fire response of a steel girder bridge," *Journal of Constructional Steel Research*, vol. 75, pp. 93–103, 2012.

[5] V. Kodur, E. Aziz, and M. Dwaikat, "Evaluating fire resistance of steel girders in bridges," *Journal of Bridge Engineering*, vol. 18, no. 7, pp. 633–643, 2013.

[6] A. Astaneh-Asl, C. R. Noble, J. Son, A. P. Wemhoff, M. P. Thomas, and L. D. McMichael, "Fire protection of steel bridges and the case of the macarthur maze fire collapse," in *Proceedings of the ASCE Technical Council on Lifeline Earthquake Engineering in a Multihazard Environment Conference (TCLEE '09)*, pp. 726–737, Oakland, Calif, USA, July 2009.

[7] *Structural Steel for Bridge*, GB/T 714-2008, Standards Press of China, Beijing, China, 2008.

[8] T. T. Lie, "Fire resistance of circular steel columns filled with bar-reinforced concrete," *Journal of Structure Engineering*, vol. 120, no. 8, pp. 75–88, 1993.

[9] T. T. Lie and B. Celikkol, "Method to calculate the fire resistance of circular reinforced concrete columns," *ACI Materials Journal*, vol. 88, no. 1, pp. 84–91, 1991.

[10] H.-Y. Zhang and W.-Z. Zheng, "Mechanical property of steel strand at high temperature," *Journal of Harbin Institute of Technology*, vol. 39, no. 6, pp. 861–865, 2007.

[11] Z. Yan and H. Zhu, "Study on fire scenario and fire safety of tunnel lining," *Chinese Journal of Underground Space and Engineering*, vol. 2, no. 8, pp. 1320–1325, 2006.

[12] H. Ingason and A. Lönnermark, "Heat release rates from heavy goods vehicle trailer fires in tunnels," *Fire Safety Journal*, vol. 40, no. 7, pp. 646–668, 2005.

[13] H. Ingason, "Fire growth rate is more important than maximum heat release rate in tunnel fires," in *Tunnel Management International*, pp. 669–673, Mälardalens Högskola, Akademin för Hallbar Samholloch Teknikutveckling, 2006.

[14] J. Alos-Moya, I. Paya-Zaforteza, M. E. M. Garlock, E. Loma-Ossorio, D. Schiffner, and A. Hospitaler, "Analysis of a bridge failure due to fire using computational fluid dynamics and finite element models," *Engineering Structures*, vol. 68, pp. 96–110, 2014.

[15] S. P. Timoshenko, *Theory of Elastic Stability*, McGraw-Hill International Book, New York, NY, USA, 1985.

[16] P. Wang, C. Liu, M. Liu, and X. Wang, "Numerical studies on large deflection behaviour of axially restrained corrugated web steel beams at elevated temperatures," *Thin-Walled Structures*, vol. 98, pp. 58–74, 2016.

[17] J. Vácha, P. Kyzlík, I. Both, and F. Wald, "Beams with corrugated web at elevated temperature, experimental results," *Thin-Walled Structures*, vol. 98, pp. 19–28, 2016.

[18] ANSYS, *User's Manual. Multiphysics 14.0*, ANSYS, Canonsburg, Pa, USA, 2011.

[19] China Communications Press, "General code for design of highway bridges and culverts," JTG D60-2004, China Communications Press, Beijing, China, 2004.